Optical pulse compression*

D. Grischkowsky

IBM Thomas J. Watson Research Center, Yorktown Heights, New York 10598
(Received 19 August 1974)

Dramatic and controllable reshaping of frequency-modulated dye laser pulses has been observed. The pulses, nearly resonant with the $^2P_{1/2}$ line (7948 Å) of Rb, first passed through a $LiNbO_3$ frequency modulator, and then through a cell containing dilute Rb vapor where the reshaping took place. Large pulse compressions were obtained with only 400 MHz of frequency modulation due to the extremely large frequency dispersion of the group velocity.

Most of the compression schemes for optical pulses have been based on the ideas of chirp radar,[1-8] i.e., a frequency-modulated pulse is passed through a frequency-dispersive linear delay line so that the rear of the pulse catches up with the front. For the best case the resulting pulse width is limited to the reciprocal of the angular frequency bandwidth. However, the dispersion of the group velocity v_g is relatively small for the nonresonant systems proposed to date. This in turn requires a relatively large amount of frequency modulation to substantially compress nsec pulses. For pulses whose frequency is quite close to that of an atomic transition, the interaction between the light and the atoms is strong and can result in extremely slow and very frequency-dispersive group velocities.[9] For the experiments described in this paper v_g is of the order of $\frac{1}{5}c$ and the frequency dispersion of v_g is approximately 1000 times larger than that of the nonresonant delay lines. Consequently, the required amount of frequency modulation is reduced by 1000, and compression of nsec pulses becomes relatively easy.

To obtain reshaping and compression, the near-resonant frequency-modulated pulses were passed through a 100-cm cell containing Rb vapor at 120 °C. The experimental setup was similar to that described previously,[9] except that the input pulse was sinusoidally frequency modulated, and the modulation voltage and phase were monitored. The peak intensity of the input pulses was kept below 1 W/cm^2 to ensure that nonlinear polarization effects[9-11] in the vapor were negligible. The measured linewidth of the dye laser pulse before frequency modulation was less than 100 MHz.

Figure 1 shows a pulse series where the dispersion of v_g was controlled by varying the frequency difference $\Delta\omega$ between the frequency ω_0 of the resonance line and the carrier frequency ω of the input light, and where

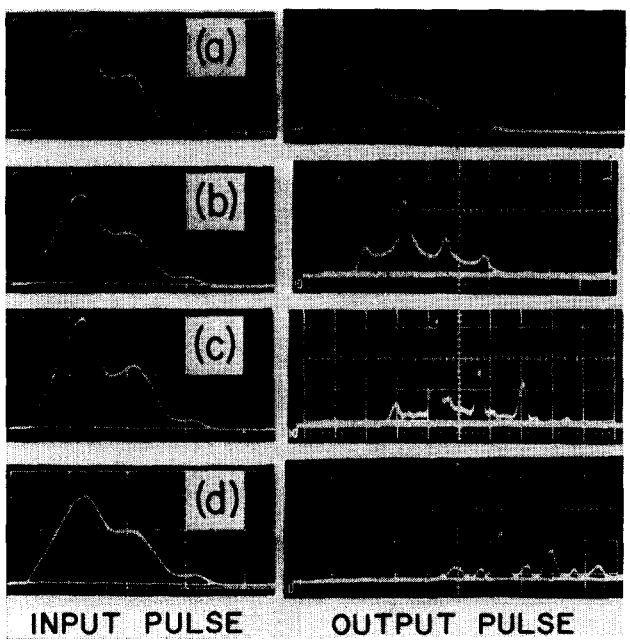

FIG. 1. Input pulses (measured with a Tektronix 519 oscilloscope at 10 nsec per large division and an ITT biplanar photodiode) to the Rb cell and the resulting output (measured with a Tektronix 7904 oscilloscope at 5 nsec per large division and an ITT biplanar photodiode). (a) $\Delta\omega/2\pi = 18.9$ GHz; $\Delta\omega = \omega_0 - \omega$, where ω_0 is the center frequency of the σ^- components of the $^2P_{1/2}$ line and ω is the constant carrier frequency of the input σ^- light. No FM. (b) $\Delta\omega/2\pi = 7.8$ GHz; $\Lambda/2\pi = 150$ MHz, where Λ is the angular modulation frequency; $(\phi_0\Lambda)/2\pi = 230$ MHz, where $(\phi_0\Lambda)/2\pi$ is the magnitude of the frequency modulation. (c) $\Delta\omega/2\pi = 6.3$ GHz; $\Lambda/2\pi = 150$ MHz; $\phi_0\Lambda/2\pi = 230$ MHz. (d) $\Delta\omega/2\pi = 5.1$ GHz; $\Lambda/2\pi = 150$ MHz; $\phi_0\Lambda/2\pi = 230$ MHz.

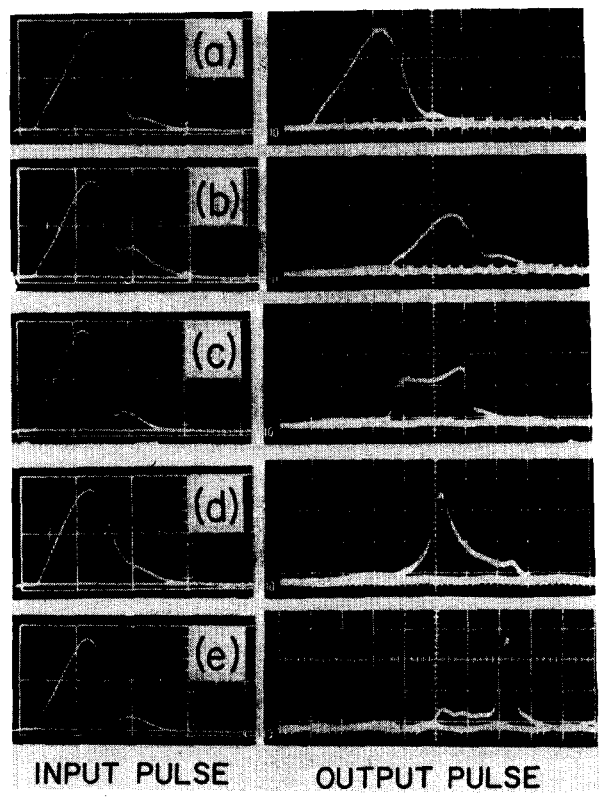

FIG. 2. Input pulses (10 nsec per large division) to the Rb cell and the resulting output (5 nsec per large division). (a) $\Delta\omega/2\pi = 19.8$ GHz; no FM. (b) $\Delta\omega/2\pi = 6.3$ GHz; no FM. (c) $\Delta\omega/2\pi = 6.3$ GHz; $\Lambda/2\pi = 90$ MHz; $\phi_0\Lambda/2\pi = 190$ MHz. (d) $\Delta\omega/2\pi = 6.3$ GHz; $\Lambda/2\pi = 90$ MHz; $\phi_0\Lambda/2\pi = 190$ MHz. (e) $\Delta\omega/2\pi = 5.1$ GHz; $\Lambda/2\pi = 90$ MHz; $\phi_0\Lambda/2\pi = 190$ MHz.

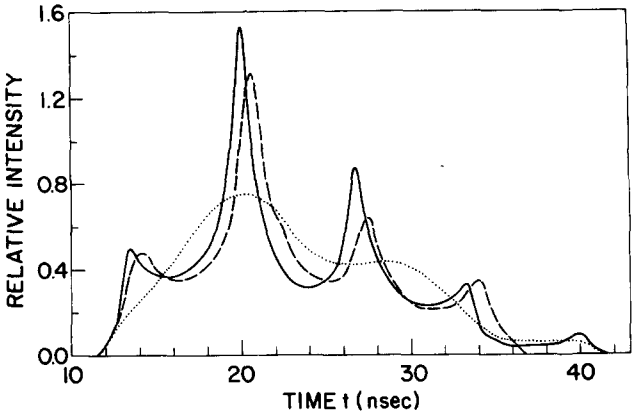

FIG. 3. Comparison between theory (solid line) and experiment (dashed line) for the output pulse of Fig. 1(b). All parameters used in the theory were measured experimentally. The dotted line, having the same shape as the input pulse, would have been the output pulse for no FM. The input pulse was normalized to unity.

the pulse width was large compared to the 6.7-nsec period of the frequency modulation (FM). Both v_g and the absorption coefficient α_0 are functions of $(\Delta\omega)^2$; when $(\Delta\omega)^2$ is reduced v_g is reduced and α_0 is increased. The dispersion of v_g can be written as $d(1/v_g)/d\omega = (2/\Delta\omega)(1/v_g - 1/c)$. Therefore, when v_g is decreased the dispersion is increased. Pulse 1(a) is an unmodulated calibration pulse relatively far off resonance with $v_g \approx c$. Hence, the start of the output pulse provides a time maker against which the delays of the other pulses may be measured and their group velocities determined. Because the attenuation of this pulse was negligible, the ratio of the input to the output pulse allows the attenuation of the other pulses to be determined. Also, as this pulse was not frequency modulated, it is clear that the amplitude variation of the input pulses is not related to the FM but is a characteristic of the dye laser. Pulse 1(b) is closer to the resonance line, is frequency modulated, and is markedly reshaped. The 7-nsec delay of the output pulse with respect to pulse 1(a) indicates $v_g \approx \frac{1}{3}c$. The output pulse shape is very dependent upon the phase (relative to the start of the laser pulse) of the modulation. For sinusoidal modulation the theory predicts that the output peaks should occur where the instantaneous frequency ω' is equal to the carrier frequency ω and where ω' is sweeping away from the resonance line. Consequently, the time interval between the output spikes should be equal to the 6.7-nsec modulation period which, as shown in the figure, agrees well with experiment. The intensity of the highest output spike is 1.3 times higher than the peak input intensity. Pulse 1(c) is still closer to the line, as indicated by the larger delay of 13 nsec, corresponding to $v_g \approx \frac{1}{5}c$, and the stronger reshaping. The measured width of the output spikes is approximately equal to the 1-nsec detector rise time. The intensity of the highest spike is 1.5 times higher than the peak input intensity even though the 13-nsec delay implies an attenuation of 0.63 (see Ref. 9). It is clear that most of the output energy is in the spikes. Pulse 1(d) shows the breakup which occurs if $\Delta\omega$ is further reduced. The output spikes have broadened and their separation is no longer equal to the FM period.

Figure 2 shows another pulse series, where the input pulse width is now of the order of the 11.1-nsec FM period. Pulse 2(a) is an unmodulated calibration pulse. Pulse 2(b) was nearer to the resonance line as shown by the 13-nsec delay corresponding to $v_g \approx \frac{1}{5}c$. As this pulse was not frequency modulated the output was not reshaped. However, the 13-nsec delay implies an attenuation factor of 0.63, which agrees well with the value 0.6 obtained from the figure. Pulses 2(c) and 2(d) had the same frequency offset as 2(b) but were frequency modulated. Consequently, the output pulse shapes differ from the input. It is interesting that the output pulses 2(c) and 2(d) are quite different, even though both input pulses were very similar. This is explained by the phase difference of π between the FM of the two pulses. For pulse 2(c) the zero crossings, corresponding to the positions where the output spikes would form, straddled the input pulse and led to a buildup of the edges and a depression of the pulse peak. In contrast, for pulse 2(d), a zero crossing reasonably near the pulse peak caused the peak to grow and the pulse to sharpen. Pulse 2(e) shows the compression of a 10-nsec input pulse to a 2-nsec output pulse.

A simple way of understanding these results is to recall[10,11] that, to a reasonably good approximation, both the energy and the instantaneous frequency travel with the group velocity. Consequently every point on the pulse envelope can be distinguished by its instantaneous frequency. As the pulse propagates through the vapor, the frequency dispersion of the group velocity causes the points to move closer together or further apart. Because energy does not flow past any of these conceptual points, if the points move closer together the intensity goes up, and if the points move further apart the intensity goes down. This process goes on until two points overlap and an intersection is reached.

The above intuitive argument summarizes the main features of the analytic solution

$$\mathcal{E}^2(\tau, z) = \exp(-\alpha_0 z)\mathcal{E}_0^2(\tau)\left[1 + z\frac{d\omega'}{d\tau}\left(\frac{\partial}{\partial\omega'}\ \frac{1}{v_g}\right)\right]^{-1} \qquad (1)$$

which was reported at the Eighth IEEE Quantum Electronics Conference.[12] α_0 is the linear absorption coefficient; z is the cell length; $\mathcal{E}_0^2(\tau)$ is the input pulse shape at $z = 0$; $\tau = t - z/v_g$ is the reduced time; $\omega' = \omega + \partial\phi/\partial t$ is the instantaneous angular frequency; ω is the constant carrier frequency; $\phi = \phi_0 \sin(\Lambda\tau + \eta)$ is the time-dependent phase angle due to the $LiNbO_3$ modulator; ϕ_0 is the amplitude of the phase modulation; Λ is the angular modulation frequency; η is the initial phase angle. Given τ and z, the corresponding time t can be calculated. In other words $\mathcal{E}^2(\tau, z) = \mathcal{E}^2(t, z)$, where t is obtained from the relationship $t = \tau + z/v_g$. For Eq. (1) the adiabatic following model $(AF)^{9-11}$ in the low-intensity limit is used for the electric susceptibility. Equation (1) is the low-intensity solution of Eqs. (41a), and (41b) of Ref. 10, and of Eqs. (2a), and (2b) of Ref. 11 with finite T_2. The solution agrees to within a few percent with the predictions of linear dispersion theory (LDT) for modest amounts of reshaping such as depicted in

Fig. 1(b). A detailed comparison between Eq. (1) and the results of LDT will be presented in a more extensive future publication.

Equation (1) is compared with experiment in Fig. 3, where all the required parameters were measured experimentally and the hyperfine splitting of Rb was included in the theory. The agreement between theory and experiment is good. These results amply demonstrate the marked controllable reshaping which can be obtained with only about 400 MHz of frequency modulation. The sinusoidal frequency modulation is not optimal for pulse compression but was chosen as a convenient example. By optimizing the frequency sweep it should be relatively easy to obtain bandwidth-limited output pulses.

The results of Fig. 1 demonstrate that if a cw laser were used the output would consist of a train of identical pulses separated by the FM period with the pulse width determined by the FM strength. As the modulation frequency could be precisely controlled, for a constant frequency the output would constitute an optical clock or for a time-dependent frequency the pulse separation would be time dependent. Pulsed RF modulation would produce pulse bursts from the cell. As shown by the difference between Figs. 2(c) and 2(d), changing the phase of the modulation allows the peak of the output pulse to be placed anywhere on the output envelope and many desired pulse shapes can be produced.

The author would like to acknowledge that his initial interest in this problem was promoted by suggestions from Eric Courtens and J.A. Armstrong. Michael M.T. Loy provided a numerical solution to the Bloch equations against which AF and LDT were compared. R.J. Bennett made many important contributions to this work. Useful discussions were held with R.K. Bullough, P.P. Sorokin, and J.J. Wynne.

*Work partially supported by ONR under Contract No. N0014-70-C-0187.

[1]J.R. Klauder, A.C. Price, S. Darlington, and W.J. Albersheim, Bell Syst. Tech. J. **39**, 745 (1960).
[2]F. Gires and P. Tournois, C.R. Acad. Sci. (Paris) **258**, 6112 (1964).
[3]J.A. Giordmaine, M.A. Duguay, and J.W. Hansen, IEEE J. Quantum Electron. **QE-4**, 252 (1968).
[4]E.B. Treacy, Phys. Lett. **28A**, 34 (1968).
[5]M.A. Duguay and J.W. Hansen, Appl. Phys. Lett. **14**, 14 (1969).
[6]R.A. Fisher, P.L. Kelley, and T.K. Gustafson, Appl. Phys. Lett. **14**, 140 (1969).
[7]A. Laubereau, Phys. Lett. **29A**, 539 (1969).
[8]R.A. Fisher and W. Bischel, Appl. Phys. Lett. **23**, 661 (1973).
[9]D. Grischkowsky, Phys. Rev. A **7**, 2096 (1973).
[10]D. Grischkowsky, in *Laser Applications to Optics and Spectroscopy*, Vol. II of *Physics of Quantum Electronics series*, edited by S.F. Jacobs, M. Sargent III, and M.O. Scully (Addison-Wesley, Reading, Mass., 1974).
[11]D. Grischkowsky, Eric Courtens, and J.A. Armstrong, Phys. Rev. Lett. **31**, 422 (1973).
[12]D. Grischkowsky, 1974 *International Quantum Electronics Conference, Digest of Technical Papers* (IEEE, New York, 1974), p. 47.

Accumulation-mode charge-coupled device

Richard D. Nelson

Rockwell International, Anaheim, California 92803
(Received 10 June 1974)

An accumulation-mode charge-coupled device has been fabricated and operated at 4 °K. A discussion of device energy band structure, signal-processing time, and experimental results is presented.

An accumulation-mode charge-coupled device has been fabricated and operated at 4 °K. Accumulation-mode operation is defined herein by a biasing of an MIS structure[1] which gives the same majority carrier type at the semiconductor surface as in the semiconductor bulk. The applied gate voltage is then just the negative of that used for the more usual inversion-mode MIS devices (e.g., MOSFET's, CCD's, CID's).

The nececessary condition for device operation is that the density of majority carriers in the semiconductor be small enough to provide a surface charge density small enough to be manipulated by the CCD concept. For continuous device operation with a steady-state substrate current, the maximum majority carrier density as obtained from Eq. (6) is

$$n_{max} < X_s C_i f_c / e\mu N, \tag{1}$$

where X_s is the substrate thickness, C_i the insulator capacitance, f_c the chip frequency (reciprocal of storage time per cell), e the electronic charge, μ the majority carrier mobility, and N the number of cells of delay. This criterion is satisfied for silicon only at reduced temperatures. Semiconductor substrates with wider band gaps, such as gallium arsenide, can satisfy Eq. (1) at room temperature and can, therefore, be used without cooling as substrates for accumulation-mode devices.

With the appropriate device structure, the accumulation-mode CCD can be used for the same signal-processing applications as the inversion-mode CCD. Probably the most natural application is a self-scanned infrared imager/detector. An accumulation-mode device is actually required for this application because photon absorption ($E_{impurity} < h\nu < E_{gap}$) in an extrinsic material[2] generates only one carrier type, viz., the bulk majority carrier. Figure 1 is a sketch illustrating photon detection.

